Research Square

Preprints are preliminary reports that have not undergone peer review.
They should not be considered conclusive, used to inform clinical practice,
or referenced by the media as validated information.

Condition-Dependent Corrosion Responses of L415 Pipeline Steel under SRB-Inoculated and Sterile Conditions: Effects of pH, Chloride, and Sulfate

Yi Liu

2104516150@qq.com

China Oil and Gas Pipeline Network Corporation (PipeChina), Hubei Branch

Fei Li

China Oil and Gas Pipeline Network Corporation (PipeChina), Hubei Branch

Wei Cui

China Oil and Gas Pipeline Network Corporation (PipeChina), Hubei Branch

Junyi Wei

China Oil and Gas Pipeline Network Corporation (PipeChina), Hubei Branch

Research Article

Keywords: L415 pipeline steel, sulfate-reducing bacteria, microbiologically influenced corrosion, polarization, EIS, surface heterogeneity

Posted Date: November 16th, 2026

DOI: https://doi.org/10.21203/rs.3.rs-11525832/v1

License: This work is licensed under a Creative Commons Attribution 4.0 International License.
Read Full License

Additional Declarations: No competing interests reported.

Condition-Dependent Corrosion Responses of L415 Pipeline Steel under SRB-Inoculated and Sterile Conditions: Effects of pH, Chloride, and Sulfate

Yi Liu [1*], Fei Li [1], Wei Cui [1] and Junyi Wei [1]

[1] China Oil and Gas Pipeline Network Corporation (PipeChina), Hubei Branch; Wuhan 430070, China
* Correspondence: 2104516150@qq.com

Abstract

Environmental changes reshape the corrosion contrast between SRB-inoculated steel and its sterile reference. L415 pipeline steel was evaluated across separate pH, nominal chloride, and supplemental-sulfate series using gravimetry, polarization, impedance, and surface observations. Inoculated gravimetric corrosion rates peaked at pH 6.6, but agreement between mass loss and fitted current densities depended on the condition: inoculated loss was lower at pH 4.6 despite near-equal currents, and higher at pH 8.0 despite a lower current. In the chloride series, the inoculated-to-sterile current-density ratio decreased from 15.51 at 3000 mg/L to 0.25 at 12000 mg/L. This variation involved both a declining inoculated response and a rising sterile response; the highest-label gravimetric rate difference remained small. Inoculated mass loss increased across the sulfate labels, while the sterile reference exhibited an intermediate minimum. The principal finding is that environmental dependence emerges from the trajectories of both exposure groups and from their correspondence across indicators. Together, the environmental comparisons identify where cumulative loss, fitted electrochemistry and local surface appearance converge or diverge, extending the earlier temporal characterization of L415 steel.

Keywords: L415 pipeline steel; sulfate-reducing bacteria; microbiologically influenced corrosion; polarization; EIS; surface heterogeneity

1. Introduction

Buried pipeline steel is exposed to soil environments in which acidity, dissolved ions, and microbial activity can vary over short distances[1,2]. Sulfate-reducing bacteria (SRB) contribute to anaerobic iron corrosion through sulfide-associated processes and, in specific biological systems, direct electron uptake. However, the presence of SRB alone does not determine the extent of metal degradation or whether an inoculated exposure will corrode more rapidly than a sterile-reference condition[3]. Environmental changes can affect both microbial processes and solution corrosivity[4]. Paired environmental comparisons therefore require assessment of both exposure-group trajectories.

Previous investigations illustrate why both exposure-group responses matter. For L415 steel at initial pH 6.4 and 8.0, Liu et al.[5] reported that varying inoculum concentration affected uniform loss and maximum localized corrosion differently. Anion effects have also been examined in an X80 steel/sea-mud system[6]. In experiments with pure iron, matching chloride concentration across two

media did not eliminate differences in SRB-associated corrosion, demonstrating the relevance of other medium constituents[7]. Together, these studies motivate paired comparisons that resolve environmental responses within a defined steel–medium system.

Interfacial corrosion products and biofilms provide a possible connection between environmental chemistry and corrosion. Iron-sulfide deposits can impede transport or participate in localized attack depending on their structure and the associated process[8,9]. Extracellular polymeric substances (EPS) interact with iron ions and have been associated with time-dependent promotion and inhibition of corrosion in cast-iron systems[10,11]. In an X80 steel/Desulfovibrio desulfuricans system, additions of purified EPS increased mass loss and fitted corrosion currents under the tested chloride conditions[12]. These observations provide an interfacial framework for interpreting condition-dependent differences in metal loss, current density and impedance[13,14].

In our previous investigation, we evaluated the temporal corrosion evolution of L415 pipeline steel in a prepared soil-simulating medium adjusted to pH 4.6, integrating biological growth, gravimetric, electrochemical, and surface measurements[15]. Electrochemistry was followed over 3–14 d, while the displayed gravimetric comparisons concerned 7 and 14 d[15]. That time-resolved characterization provides a foundation for addressing a different question: how does the relationship between inoculated and sterile-reference exposures change when environmental conditions are varied? The present study examines environmental dependence across separate pH, chloride, and supplemental-sulfate series.

Here, we evaluate how these environmental series alter L415 corrosion under inoculated exposure relative to its sterile reference, identifying where gravimetric corrosion-rate orderings correspond with fitted polarization current densities. Each series is first assessed through its within-group response and same-condition contrast. Fitted current densities provide descriptive quantitative comparisons, while electrochemical impedance spectroscopy (EIS) and surface observations supply complementary electrical and spatial context. The focus is on identifying which features of the contrast arise from changes in either exposure group and which persist across measurement types. This comparison extends the earlier time-dependent findings by identifying recurring agreements and contrasts across the measured indicators.

2. Materials and Methods

2.1. Material and specimens

In this study, L415 pipeline steel was selected as the research material, and its chemical composition is presented in **Table 1**. The metallographic microstructure of the as-received L415 pipeline steel is shown in **Figure 1**. For the immersion mass-loss corrosion tests, sheet specimens measuring 40 mm × 13 mm × 2 mm were fabricated by wire electrical discharge machining, and a hole was drilled at the upper end of each specimen. The specimen surfaces were then ground sequentially with 400#, 600#, 800#, 1000#, and 1200# waterproof abrasive papers and numbered accordingly. After grinding, the specimens were rinsed with deionized water, dehydrated with absolute ethanol, and dried with cold air. Prior to the experiments, all prepared specimens were sterilized under ultraviolet light for 30 min to prevent contamination.

For the electrochemical tests, square specimens measuring 10 mm × 10 mm × 3 mm were prepared by wire electrical discharge machining. A copper wire was welded securely to one side of each specimen, after which the specimen was encapsulated with epoxy resin, leaving a working area of 10 mm × 10 mm exposed on the opposite side. The encapsulated specimens were sequentially ground with 400# to 1200# waterproof abrasive papers. Subsequently, the specimens were rinsed with deionized water, dehydrated with absolute ethanol, and dried before use.

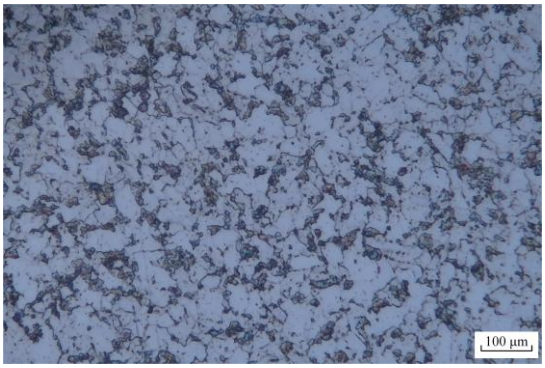


Figure 1. Metallographic microstructure of L415 pipeline steel

Table 1. Chemical composition of L415 pipeline steel

	C	Cr	Mn	Ni	Mo	Fe
L415	**0.0552**	**0.0429**	**0.5597**	**—**	**—**	**Bal.**

2.2. Preparation of the SRB Inoculum and Simulated Soil Solution

Soil samples were collected from the vicinity of buried pipelines in the Gannan region of Jiangxi Province, China. An SRB strain was obtained from these field samples through enrichment, isolation, and purification, and Postgate's C medium **Table 3** was used for strain cultivation. A simulated soil solution was formulated according to the physicochemical properties of the collected soil samples **Table 3** to reproduce the local soil environment. The simulated soil solution was then mixed with Postgate's C medium at a volume ratio of 9:1. The pH of the mixture was adjusted to 4.6 with 4 wt% NaOH and 4 wt% acetic acid solutions. Subsequently, the mixture was heat-sterilized and purged with N_2 for 2 h to remove dissolved oxygen. Once the mixture had cooled naturally to room temperature, the sterile medium was inoculated with an SRB suspension at 5% (v/v). This procedure yielded the SRB-containing simulated Gannan soil solution used in the corrosion tests.

Table 2. Soil-simulating solution

Reagent	Reported amount (g/L)
$MgCl_2·6H_2O$	0.3800
$CaCl_2$	0.6500
KCl	0.0350
$NaNO_3$	0.2000
$Na2SO_4$	0.2130
$NaHCO_3$	0.2268

Table 3. Postgate C enrichment medium

Reagent	Formula	Reported amount (g/L)
Potassium dihydrogen phosphate	KH_2PO_4	0.5
Ammonium chloride	NH_4Cl	1.0
Sodium sulfate	Na_2SO_4	1.0
Calcium chloride	$CaCl_2$	0.05
Magnesium chloride hexahydrate	$MgCl_2·6H_2O$	2.0
Yeast extract		1.0
Ascorbic acid	$C_6H_8O_6$	0.1
Sodium thioglycolate	$C_2H_3NaO_2S$	0.1
Ferrous sulfate heptahydrate	$FeSO_4·7H_2O$	0.5
Sodium D-lactate	$C_3H_5NaO_3$	1.1

2.3. Weight-loss corrosion test

The average corrosion rate of L415 pipeline steel was determined by mass-loss measurements. Before immersion, the prepared sheet specimens measuring 40 mm × 13 mm × 2 mm were rinsed with deionized water, dehydrated with absolute ethanol, dried, and weighed using an electronic analytical balance. The initial mass of each specimen was recorded as m_0. The specimens were then immersed for 14 d in sterile or SRB-containing simulated soil solutions with different pH values, Cl^- concentrations, and SO_4^{2-} concentrations.

After immersion, the specimens were removed from the test solutions, and the corrosion products were chemically cleaned according to ASTM G1-03. Briefly, the corroded specimens were immersed for 10 min at room temperature in a cleaning solution composed of 500 mL hydrochloric acid, 500 mL distilled water, and 3.5 g hexamethylenetetramine. The cleaned specimens were then rinsed with distilled water and absolute ethanol, dried, and reweighed to obtain the final mass m_1. The average corrosion rate was calculated using the following equation:

$$v=\frac{87600\times(m_0-m_1)}{\rho A t} \quad (1)$$

where V is the average corrosion rate in $mm·a^{-1}$, m_0 and m_1 are the specimen masses before immersion and after corrosion-product removal in g, respectively, ρ is the density of L415 steel in $g·cm^{-3}$, A is the exposed surface area in cm^2, and t is the immersion time in h. At least three parallel specimens were tested under each condition, and the average values were reported.

2.4. Electrochemical measurement

All electrochemical tests were performed in the simulated soil solution at room temperature using a CHI760E electrochemical workstation (Shanghai Chenhua, Shanghai, China). A conventional three-electrode arrangement was used in all measurements. The working electrode (WE) was an epoxy-embedded steel specimen with an exposed area of 1.0 cm2; a platinum sheet and a saturated calomel electrode (SCE) served as the counter electrode (CE) and reference electrode (RE), respectively. Unless otherwise specified, all potentials reported in this study are referenced to the SCE.

Before each test, the working electrode was immersed in the test solution for 60 min, and its open-circuit potential (OCP) was monitored until it stabilized. The OCP was considered stable when the potential variation was less than 2 mV over a 10 min period. After this stability criterion was met, potentiodynamic polarization curves (PDP) were recorded by scanning the potential from −0.25 to +0.25 V versus the OCP at a scan rate of 0.5 mV/s. Electrochemical impedance spectroscopy measurements were conducted at the OCP over a frequency range of 100 kHz to 10 mHz with a sinusoidal perturbation amplitude of 10 mV. The impedance spectra were fitted and analyzed using ZSimpWin software. At least three independent measurements were performed under each experimental condition to ensure reproducibility.

2.5. Microscopic characterization

The L415 steel specimens were removed from the simulated soil solution and gently rinsed with deionized water. Corrosion products were then chemically removed in accordance with ASTM G1-03 . Briefly, the corroded specimens were immersed for 10 min at room temperature in a cleaning solution composed of 500 mL hydrochloric acid, 500 mL distilled water, and 3.5 g hexamethylenetetramine. After descaling, the specimens were sequentially rinsed with distilled water and anhydrous ethanol and then dried. Metallographic microscopy was used to examine the general corrosion morphology and spatial distribution of localized corrosion on the cleaned steel surfaces.

3. Results and Discussion

3.1. Mass-Loss Results of L415 Pipeline Steel in Simulated Soil Solutions

Gravimetric measurements across the pH series (**Figure 2**) demonstrate that solution acidity fundamentally governs whether SRB accelerate or retard L415 pipeline steel dissolution. Under sterile conditions, raising the electrolyte pH from 4.6 to 8.0 drove a monotonic decline in the corrosion rate from 0.194 to 0.072 $mm \cdot a^{-1}$ as reducible H^+ ions were progressively depleted. Bacterial inoculation disrupted this linear decay: the corrosion rate peaked at 0.183 $mm \cdot a^{-1}$ at pH 6.6 before subsiding to 0.146 $mm \cdot a^{-1}$ at pH 8.0. Notably, abiotic dissolution at pH 4.6 outpaced that in the SRB-containing medium, where intense proton reduction dominated cathodic kinetics while acidic stress constrained microbial metabolism. Once the electrolyte shifted toward circumneutral and mildly alkaline regimes, diminished proton reduction coincided with vigorous SRB metabolic activity, turning biocatalytic sulfate reduction into the primary driver of metal loss.

Varying the chloride concentration triggered opposite non-monotonic trajectories between the inoculated and abiotic electrolytes. In the SRB-containing medium, mass loss climbed from 0.203 $mm \cdot a^{-1}$ at 600 mg/L Cl^- to an apex of 0.229 $mm \cdot a^{-1}$ at 3000 mg/L, but retreated to 0.179 $mm \cdot a^{-1}$ as salinity reached 12000 mg/L. The sterile baseline followed an inverted profile: dissolution subsided from 0.153 to 0.110 $mm \cdot a^{-1}$ between 500 and 6000 mg/L Cl^- before surging to 0.191 $mm \cdot a^{-1}$ at 12000 mg/L. Moderate chloride levels thus amplified microbially influenced degradation, whereas extreme salinity suppressed bacterial activity while promoting aggressive Cl^- penetration through the abiotic surface film.

Unlike the non-monotonic response to chloride, the corrosion rate in the SRB-containing system increased nearly monotonically with sulfate concentration, from 0.146 $mm \cdot a^{-1}$ in the sulfate-free solution to 0.213 $mm \cdot a^{-1}$ at 9000 mg/L SO_4^{2-}. Under sterile conditions, the rate instead decreased from 0.192 $mm \cdot a^{-1}$ in the sulfate-free solution to 0.080 $mm \cdot a^{-1}$ at 3000 mg/L SO_4^{2-}, before increasing to 0.147 $mm \cdot a^{-1}$ at 9000 mg/L.

Overall, SRB substantially increased the corrosion rate of L415 steel under near-neutral and sulfate-rich conditions. However, strongly acidic and extremely chloride-rich environments could

mask or even exceed the biological contribution to corrosion. These findings demonstrate that the microbiologically influenced corrosion of L415 pipeline steel is governed by the coupled effects of SRB metabolism and the physicochemical characteristics of the simulated soil solution.

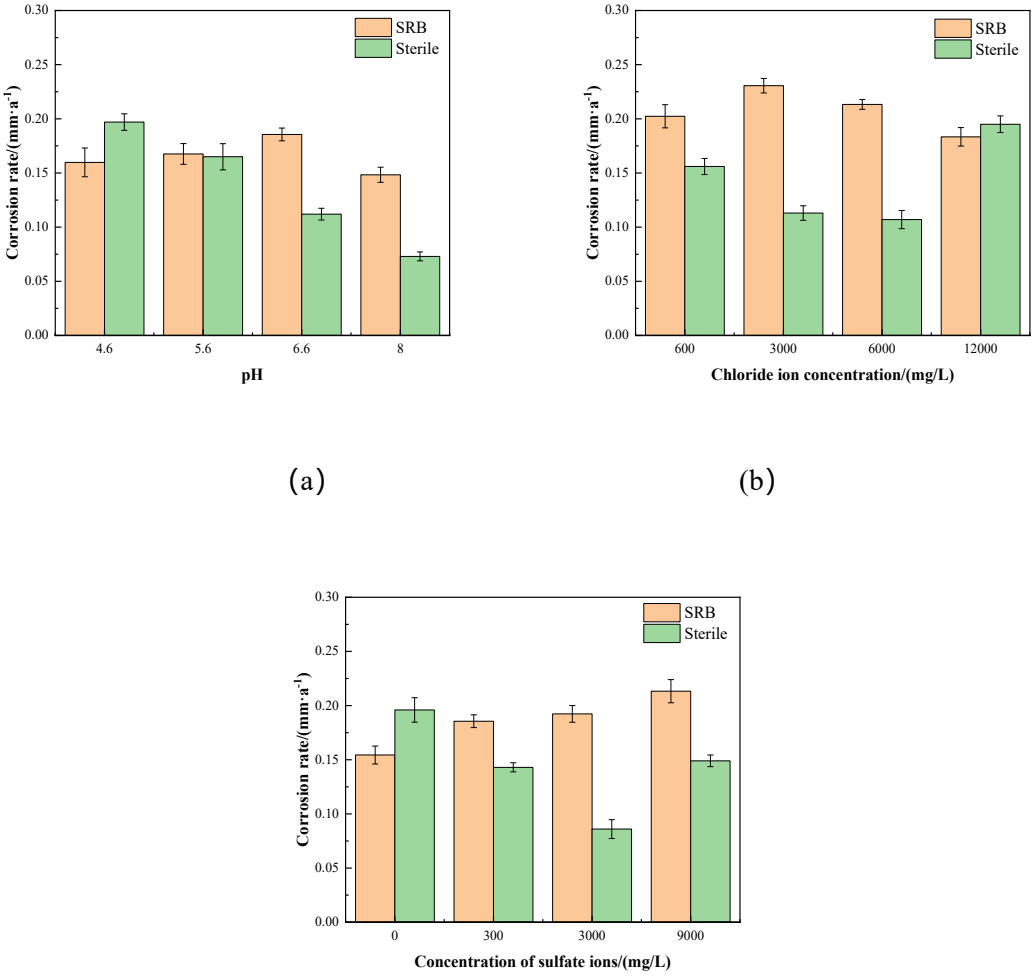


Figure 2. Mass-loss corrosion rates of L415 pipeline steel after 14 d of immersion in SRB-containing and sterile simulated soil solutions under different (a) pH , (b) chloride concentrations, and (c) sulfate concentrations.

3.2. PDP Results of L415 Pipeline Steel in Simulated Soil Solutions

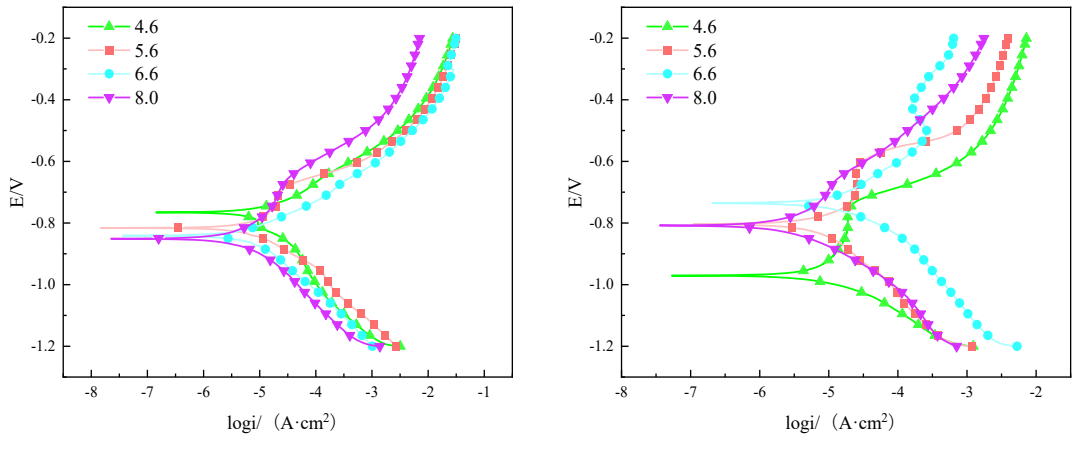
The fitted polarization parameters indicate that the corrosion kinetics of L415 pipeline steel were governed by the combined effects of SRB and solution chemistry. As shown in **Figure 3** a, In the sterile solutions, increasing the pH from 4.6 to 8.0 shifted E_{corr} negatively from −0.766 to −0.851 V, while i_{corr} decreased from 1.512×10^{-5} to 5.962×10^{-6} A·cm^{-2}. This trend suggests that increasing pH suppressed proton-involved cathodic reactions and reduced the overall corrosion kinetics. In the SRB-containing solution at pH 4.6, E_{corr} shifted to −0.971 V, approximately 205 mV more negative than that in the sterile solution, whereas the corresponding i_{corr} values were nearly identical. This discrepancy indicates that the negative shift in E_{corr} reflected changes in interfacial electrochemical reactions rather than an increase in corrosion rate. At pH 6.6, the SRB-containing system exhibited

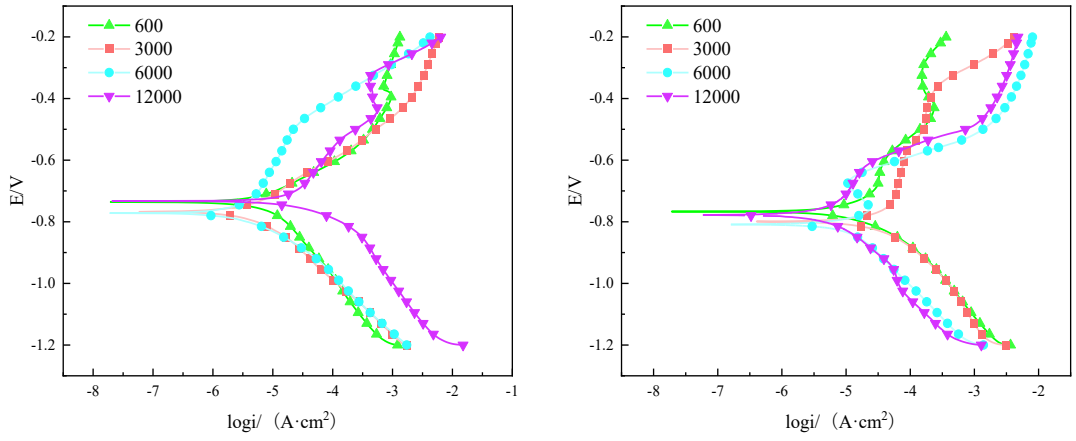
the highest i_{corr} of 1.708 × 10^{-5} A·cm^{-2}, approximately 2.53 times that of the sterile system, indicating that near-neutral conditions were more favorable for SRB-associated corrosion. At pH 8.0, however, i_{corr} decreased to 3.942 × 10^{-6} A·cm^{-2}, which may be related to the barrier effect of the biofilm and corrosion-product layer under alkaline conditions.

Potentiodynamic polarization revealed non-monotonic yet diverging kinetic responses to chloride across the two media. Under abiotic conditions, i_{corr} subsided from 8.423 × 10^{-6} A·cm^{-2} at 600 mg/L Cl^- to 4.334 × 10^{-6} A·cm^{-2} at 6000 mg/L, before surging nearly an order of magnitude to 3.898 × 10^{-5} A·cm^{-2} at 12000 mg/L; this jump coincided with a pronounced rightward shift of the cathodic branch, reflecting chloride-induced film rupture and localized attack at extreme salinity. Inoculated electrodes followed an opposing trajectory: i_{corr} rose from 2.384 × 10^{-5} A·cm^{-2} at 600 mg/L to an apex of 7.402 × 10^{-5} A·cm^{-2} at 3000 mg/L—mirrored by the marked displacement of the polarization curves toward higher current densities in Figure 3d—before dropping to 9.745 × 10^{-6} A·cm^{-2} at 12000 mg/L. Relative to the sterile baseline, bacterial participation amplified i_{corr} by 2.83-, 15.51-, and 4.70-fold at 600, 3000, and 6000 mg/L Cl^-, respectively. Once salinity reached 12000 mg/L, however, the inoculated i_{corr} fell to roughly one-quarter of the sterile value, as hyperosmotic stress curbed SRB electrocatalysis while abiotic chloride attack dominated interfacial dissolution.

Sulfate produced different effects in the two systems. In the sterile solutions, i_{corr} decreased from 2.275 × 10^{-5} A·cm^{-2} in the sulfate-free solution to 5.417 × 10^{-6} A·cm^{-2} at 3000 mg/L SO_4^{2-}, followed by an increase to 1.656 × 10^{-5} A·cm^{-2} at 9000 mg/L. This U-shaped variation suggests that sulfate influenced both the protectiveness of the corrosion-product layer and the ionic conductivity of the solution. In contrast, i_{corr} in the SRB-containing solutions increased monotonically from 6.215 × 10^{-7} A·cm^{-2} without sulfate to 2.384 × 10^{-5} A·cm^{-2} at 9000 mg/L, corresponding to an approximately 38-fold increase. The extremely low i_{corr} in the sulfate-free SRB system may be attributed to the limited availability of sulfate as a terminal electron acceptor, which restricted SRB metabolism, together with the possible barrier effect of the surface biofilm. Once sulfate was introduced, SRB metabolism could be sustained through sulfate reduction, potentially promoting sulfide formation and accelerating the corrosion of L415 steel.

Overall, SRB did not accelerate corrosion under all conditions. The strongest SRB-associated corrosion occurred under near-neutral pH, a moderate chloride concentration of 3000 mg/L, and sulfate-rich conditions. In contrast, limited or even inhibitory effects were observed under sulfate-free and alkaline conditions. These results demonstrate that the microbiologically influenced corrosion of L415 pipeline steel depends on the coupling between SRB metabolic activity and the physicochemical characteristics of the simulated soil solution.





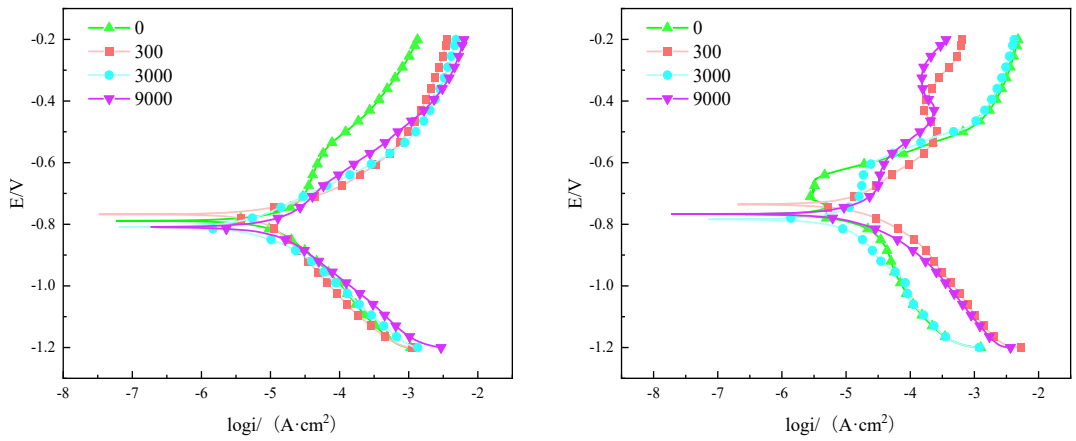


Figure 3. Potentiodynamic polarization curves of L415 pipeline steel in sterile (a, c, e) and SRB-containing (b, d, f) simulated soil solutions following 14 d of immersion: effects of pH (a, b), chloride concentration (c, d), and sulfate concentration (e, f).

Table 4. Electrochemical parameters obtained from the potentiodynamic polarization curves of L415 pipeline steel in sterile and SRB-containing simulated soil solutions.

Environmental factor	Condition	E_{corr}/V (Sterile)	i_{corr}/(A·cm^{-2}) (Sterile)	E_{corr}/V (SRB-containing)	i_{corr}/(A·cm^{-2}) (SRB-containing)
pH	4.6	−0.766	1.512×10^{-5}	−0.971	1.519×10^{-5}
pH	5.6	−0.816	1.277×10^{-5}	−0.804	1.032×10^{-5}
pH	6.6	−0.841	6.755×10^{-6}	−0.809	1.708×10^{-5}
pH	8.0	−0.851	5.962×10^{-6}	−0.808	3.942×10^{-6}
Cl^- concentration/(mg·L^{-1})	600 mg/L	−0.736	8.423×10^{-6}	−0.767	2.384×10^{-5}
Cl^- concentration/(mg·L^{-1})	3000 mg/L	−0.768	4.773×10^{-6}	−0.799	7.402×10^{-5}
Cl^- concentration/(mg·L^{-1})	6000 mg/L	−0.772	4.334×10^{-6}	−0.809	2.036×10^{-5}
Cl^- concentration/(mg·L^{-1})	12000 mg/L	−0.733	3.898×10^{-5}	−0.778	9.745×10^{-6}
SO_4^{2-} concentration/(mg·L^{-1})	0 mg/L	−0.789	2.275×10^{-5}	−0.768	6.215×10^{-7}
SO_4^{2-} concentration/(mg·L^{-1})	300 mg/L	−0.768	1.137×10^{-5}	−0.736	1.708×10^{-5}
SO_4^{2-} concentration/(mg·L^{-1})	3000 mg/L	−0.809	5.417×10^{-6}	−0.784	2.009×10^{-5}
SO_4^{2-} concentration/(mg·L^{-1})	9000 mg/L	−0.809	1.656×10^{-5}	−0.767	2.384×10^{-5}

Note: All potentials are reported versus SCE, and the i_{corr} values were obtained by Tafel fitting.

3.3. EIS Results of L415 Pipeline Steel in Simulated Soil Solutions

Figure 4 presents the Nyquist and Bode plots of L415 pipeline steel after 14 d of immersion in sterile and SRB-containing simulated soil solutions at different pH values. The corresponding equivalent circuit models are shown in **Figure 5**. The apparent diameter of the Nyquist arc and the low-frequency impedance modulus varied markedly with pH and the presence of SRB.

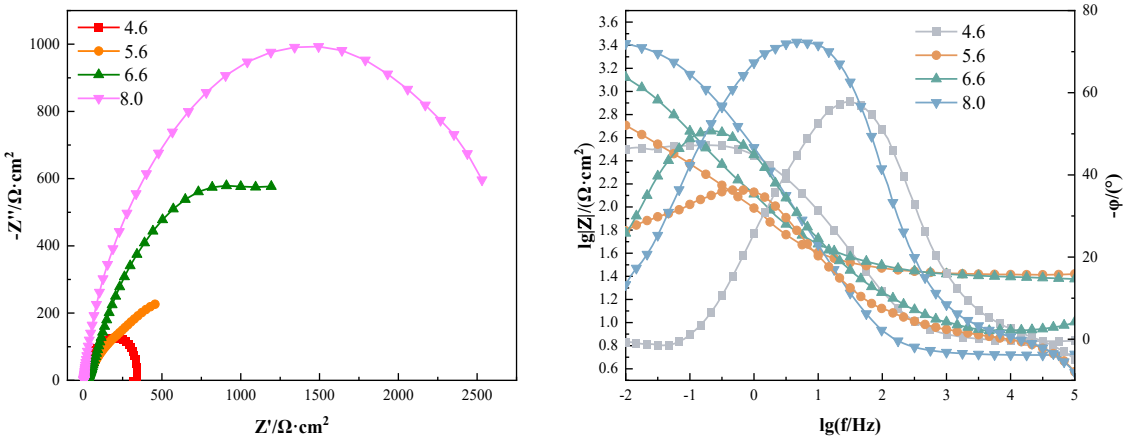
In the sterile system, both the apparent diameter of the Nyquist arc and the low-frequency impedance modulus increased with increasing pH, indicating a gradual improvement in corrosion resistance. Specifically, R_p increased from 354.6 Ω·cm^2 at pH 4.6 to 962.1 Ω·cm^2 at pH 5.6, 2675

$\Omega \cdot cm^2$ at pH 6.6, and 3024 $\Omega \cdot cm^2$ at pH 8.0. The increase in R_c from 448.6 to 1117 $\Omega \cdot cm^2$ and in R_{ct} from 513.5 to 1907 $\Omega \cdot cm^2$ suggests that the surface layer became more protective and that charge transfer was further inhibited as the pH increased.

The SRB-containing system exhibited a different pH-dependent trend. R_p decreased from 3294 $\Omega \cdot cm^2$ at pH 4.6 to 2931.41 $\Omega \cdot cm^2$ at pH 5.6 and reached a minimum of 2714.03 $\Omega \cdot cm^2$ at pH 6.6. R_p then increased markedly to 5025.1 $\Omega \cdot cm^2$ at pH 8.0. In contrast, the maximum R_p at pH 8.0 suggests that the SRB-associated biofilm and corrosion-product layer provided greater interfacial resistance under alkaline conditions, consistent with the lower i_{corr} observed in the polarization tests.

Across pH 4.6, 5.6, and 8.0, bacterial colonization elevated the fitted polarization resistance (R_p) to 9.29, 3.05, and 1.66 times the corresponding sterile values. At pH 6.6, however, the two media converged to near parity, registering 2675 $\Omega \cdot cm^2$ in the sterile solution and 2714.03 $\Omega \cdot cm^2$ in the SRB-containing medium. Although composite biofilm–FeS deposits inflated the macroscopic impedance modulus, they failed to confer uniform substrate passivation. Specifically, the coexistence of matching Rp values with an elevated inoculated i_{corr} at pH 6.6 demonstrates that surface-layer capacitance masks active, localized charge transfer occurring at unshielded anodic sites beneath the porous corrosion crust.

Overall, increasing pH continuously improved the corrosion resistance of L415 steel in the sterile solutions. In contrast, the SRB-containing system exhibited the lowest polarization resistance at pH 6.6 and the highest resistance at pH 8.0. These findings demonstrate that pH regulated not only the corrosion kinetics of L415 steel but also the structure and protectiveness of the interfacial layer formed in the presence of SRB.



(a) (b)

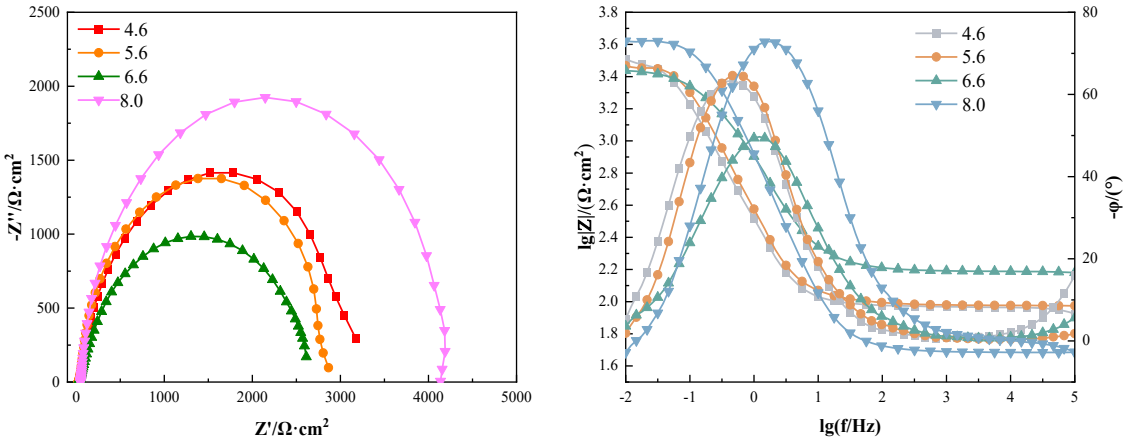


Figure 4. EIS results of L415 pipeline steel after 14 d of immersion in simulated soil solutions at different pH values: Nyquist plots (a, c) and Bode plots (b, d) for the sterile (a, b) and SRB-containing (c, d) systems.

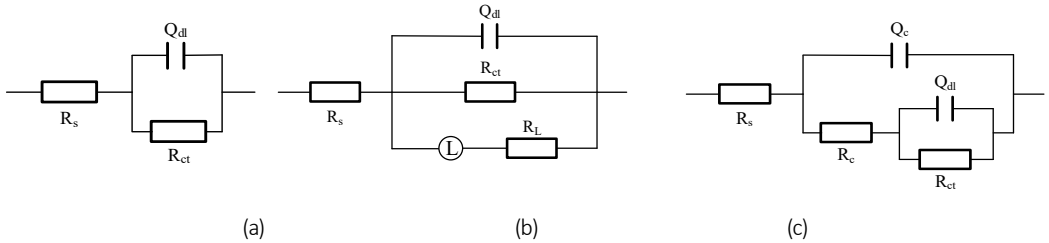


Figure 5. Equivalent circuit models used to fit the EIS data of L415 pipeline steel in sterile and SRB-containing simulated soil solutions at different pH : (a) the sterile at pH 6.6 and the SRB-containing at pH 4.6, 5.6, 6.6, and 8.0; (b) the sterile at pH 4.6; and (c) the sterile at pH 5.6 and 8.0.

Table 5. Fitted EIS parameters of L415 pipeline steel in sterile and SRB-containing simulated soil solutions at different pH values.

	pH	R_s ($\Omega\cdot cm^2$)	R_c ($\Omega\cdot cm^2$)	R_{ct} ($\Omega\cdot cm^2$)	R_L ($\Omega\cdot cm^2$)	L ($H\cdot cm^2$)	R_p ($\Omega\cdot cm^2$)
Sterile	4.6	6.85		354.6	2531	7894	354.6
	5.6	26.19	448.6	513.5			962.1
	6.6	25.55		2675			2675
	8	5.30	1117	1907			3024
SRB	4.6	37.19		3294			3294
	5.6	35.42		2931.41			2931.41
	6.6	30.00		2714.03			2714.03
	8	35.42		5025.1			5025.1

Figure 6 presents the Nyquist and Bode plots of L415 pipeline steel after 14 d of immersion in sterile and SRB-containing simulated soil solutions with different Cl^- concentrations. The corresponding equivalent circuit models are shown in **Figure 7**.

Under sterile conditions, R_p climbed progressively from 1006 $\Omega \cdot cm^2$ at 600 mg/L Cl^- through 1686 $\Omega \cdot cm^2$ at 3000 mg/L to a plateau of 1755.6 $\Omega \cdot cm^2$ at 6000 mg/L, before plunging to 548.2 $\Omega \cdot cm^2$ at 12000 mg/L. Across the 600–6000 mg/L Cl^- regime, interfacial resistance was governed almost entirely by charge-transfer resistance (R_{ct}), as surface-layer resistance (R_c) remained negligible. Raising chloride to 12000 mg/L triggered a sharp divergence between the two resistive components: R_{ct} collapsed from 1751 to 308.1 $\Omega \cdot cm^2$, while R_c surged from 4.60 to 240.1 $\Omega \cdot cm^2$. Abundant yet porous corrosion products accumulated on the steel surface at 12000 mg/L Cl^-, raising R_c while failing to impede rapid double-layer charge transfer after chloride ions penetrated the primary film to initiate localized pitting.

Inoculated electrodes traced an inverted, concave-upward R_p trajectory across the chloride gradient. From 2167.06 $\Omega \cdot cm^2$ at 600 mg/L Cl^-, R_p dipped to a nadir of 1613.45 $\Omega \cdot cm^2$ at 3000 mg/L before rebounding through 1937 $\Omega \cdot cm^2$ at 6000 mg/L to a peak of 3281 $\Omega \cdot cm^2$ at 12000 mg/L. The impedance minimum at 3000 mg/L directly mirrors the apex in polarization current density (i_{corr}), pinpointing the salinity where biogenic sulfide catalysis most severely compromises the electrical double layer; conversely, the resistive maximum at 12000 mg/L aligns with the suppressed i_{corr} observed under high-salinity inhibition.

Benchmarking the inoculated R_p against the sterile baseline further clarifies how biofilm architecture modulates interfacial impedance. The inoculated-to-sterile R_p ratio stood at 2.15 at 600 mg/L Cl^-, dipped 4.3% below the sterile reference at 3000 mg/L, and climbed to 1.10 and 5.99 at 6000 and 12000 mg/L, respectively. Only at 3000 mg/L Cl^- did a depressed R_p coincide with elevated i_{corr} to provide unambiguous electrochemical evidence of SRB-accelerated dissolution. At 600 and 6000 mg/L, the inoculated electrodes registered simultaneously higher R_p and higher i_{corr} than their sterile counterparts—a divergence arising because extracellular polymeric substances (EPS) and FeS crusts enlarge the bulk capacitive loop while sustaining localized under-deposit anodic dissolution. At 12000 mg/L, the nearly sixfold R_p advantage coupled with depressed i_{corr} confirms that compact surface fouling shielded the steel against abiotic chloride pitting.

Overall, increasing the Cl^- concentration from 600 to 6000 mg/L increased the polarization resistance of the sterile system, whereas a sharp decrease occurred at 12000 mg/L. In the SRB-containing system, the lowest polarization resistance occurred at 3000 mg/L, and the highest resistance was observed at 12000 mg/L. These results demonstrate that the effect of Cl^- on the corrosion behavior of L415 pipeline steel was strongly modified by the presence of SRB.

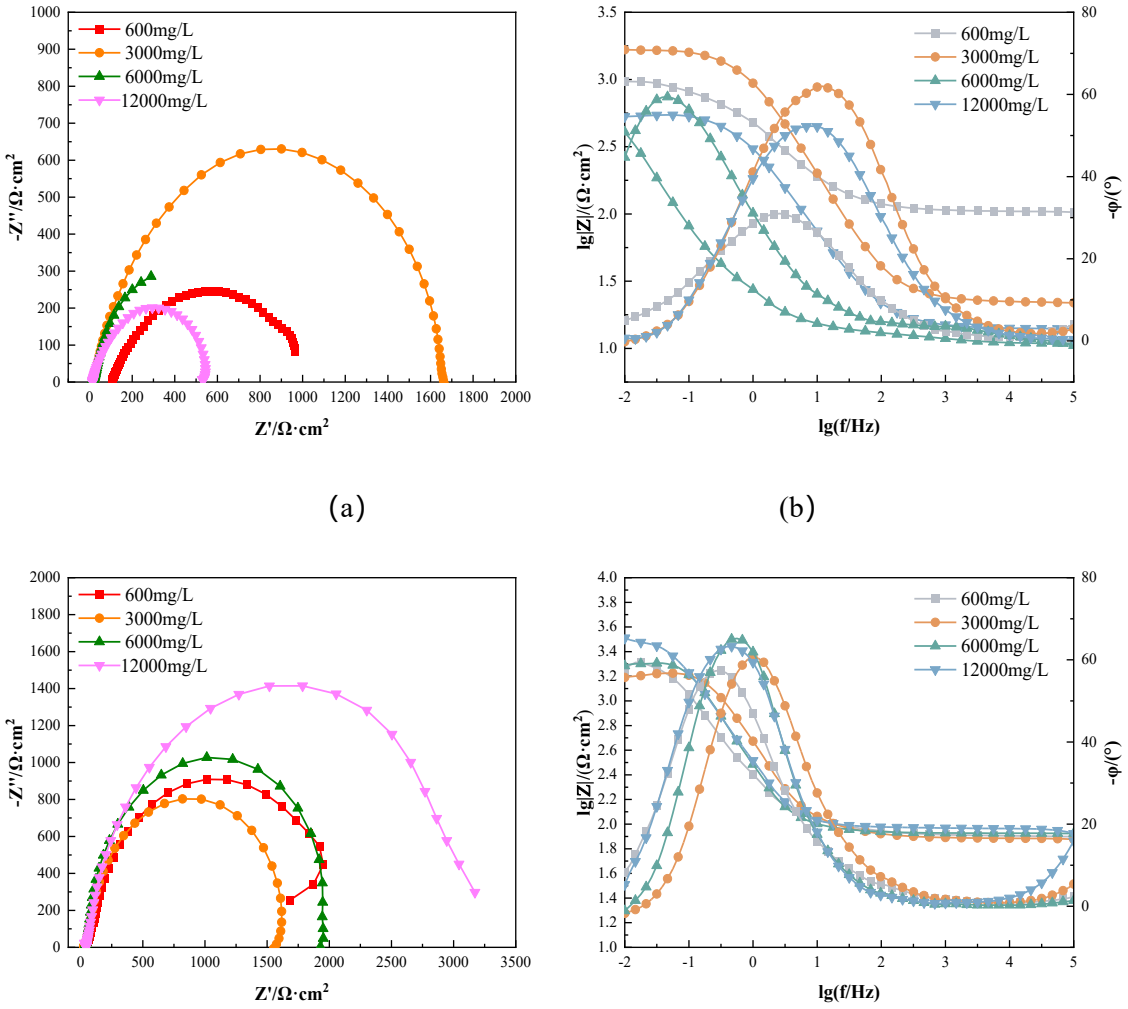


Figure 6 EIS results of L415 pipeline steel after 14 d of immersion in simulated soil solutions with different Cl⁻ concentrations: Nyquist plots (a, c) and Bode plots (b, d) for the sterile (a, b) and SRB-containing (c, d) systems.

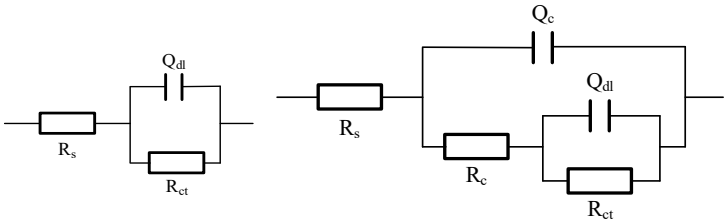


Figure 7. Equivalent circuit models used to fit the EIS data of L415 pipeline steel at different Cl⁻ concentrations under SRB-containing and sterile conditions: (a) SRB-containing system; (b) sterile.

Table 6. Fitted EIS parameters of L415 pipeline steel in sterile and SRB-containing simulated soil solutions with different chloride concentrations.

Cl⁻	R_s/(Ω·cm²)	R_c/(Ω·cm²)	R_{ct}/(Ω·cm²)	R_p/(Ω·cm²)

	concen-tration (mg/L)				
Sterile	600	90.53	17.25	989.5	1006
	3000	31.25	22.64	1664	1686
	6000	11.04	4.60	1751	1755.6
	12000	14.14	240.1	308.1	548.2
SRB	600	31.29		2167.06	2167.06
	3000	37.69		1613.45	1613.45
	6000	35.18		1937	1937
	12000	33.23		3281	3281

Figure 8 presents the Nyquist and Bode plots of L415 pipeline steel after 14 d of immersion in sterile and SRB-containing simulated soil solutions with different SO_4^{2-} concentrations. All spectra were fitted using the $R_s(Q_{dl}R_{ct})$ equivalent circuit shown in **Figure 9**. Under this circuit configuration, R_{ct} was equivalent to the total polarization resistance (R_p), allowing the impedance parameters of the sterile and SRB-containing systems to be compared directly. Rs showed no systematic dependence on SO_4^{2-} concentration and was much smaller than R_p, indicating that the changes in the impedance response were dominated by interfacial charge transfer.

In the sterile system, SO_4^{2-} produced a non-monotonic effect on the impedance response. R_p increased from 554.3 $\Omega\cdot cm^2$ in the sulfate-free solution to 961.8 $\Omega\cdot cm^2$ at 300 mg/L and reached a maximum of 1519 $\Omega\cdot cm^2$ at 3000 mg/L. R_p then decreased sharply to 562.4 $\Omega\cdot cm^2$ at 9000 mg/L. The largest Nyquist arc and the highest low-frequency impedance modulus were also observed at 3000 mg/L, which was consistent with the maximum R_p. These results suggest that a moderate SO_4^{2-} concentration increased the interfacial resistance, whereas the highest SO_4^{2-} concentration weakened this effect.

In contrast, R_p in the SRB-containing system decreased continuously as the SO_4^{2-} concentration increased. The highest R_p of 4552.80 $\Omega\cdot cm^2$ was obtained in the sulfate-free solution, whereas the value decreased to 2714.03 $\Omega\cdot cm^2$ at 300 mg/L, 2334.33 $\Omega\cdot cm^2$ at 3000 mg/L, and 2167.06 $\Omega\cdot cm^2$ at 9000 mg/L. This concentration dependence differed markedly from the non-monotonic behavior of the sterile system. The decrease in R_p was consistent with the gradual increase in i_{corr} observed in the polarization measurements, indicating that SO_4^{2-} promoted the electrochemical corrosion of L415 steel in the presence of SRB.

The contrasting sulfate dependence can be attributed to the different roles of SO_4^{2-} in the two systems. In the sterile system, moderate SO_4^{2-} concentrations appeared to increase the resistance of the interfacial layer, while a further increase to 9000 mg/L reduced the corrosion resistance. In the SRB-containing system, SO_4^{2-} can act as a terminal electron acceptor for sulfate reduction. The progressive decrease in R_p with increasing SO_4^{2-} concentration therefore suggests that sulfate availability facilitated SRB metabolism and enhanced the interfacial electron-transfer process. The particularly high R_p in the sulfate-free SRB system may indicate that the absence of SO_4^{2-} restricted SRB metabolic activity and reduced the rate of charge transfer.

Although the SRB-containing system exhibited higher absolute R_p values than the sterile system at all sulfate concentrations, its internal concentration-dependent trend still indicated a clear sulfate-promoted corrosion effect. Therefore, a higher absolute R_p should not be interpreted as uniform corrosion protection in the SRB-containing system. Instead, the continuous decrease in R_p with increasing SO_4^{2-} concentration demonstrates that sulfate availability progressively reduced the interfacial resistance and promoted SRB-associated corrosion.

Overall, SO_4^{2-} exerted a concentration-dependent but fundamentally different influence on the sterile and SRB-containing systems. In the sterile system, the maximum polarization resistance occurred at 3000 mg/L SO_4^{2-}, followed by a substantial decrease at 9000 mg/L. In the SRB-containing system, the polarization resistance decreased continuously over the entire sulfate concentration range. These results indicate that SO_4^{2-} acted primarily as an electrolyte component influencing the surface layer in the sterile system, whereas it served as a biologically available electron acceptor that promoted SRB-associated corrosion in the inoculated system.

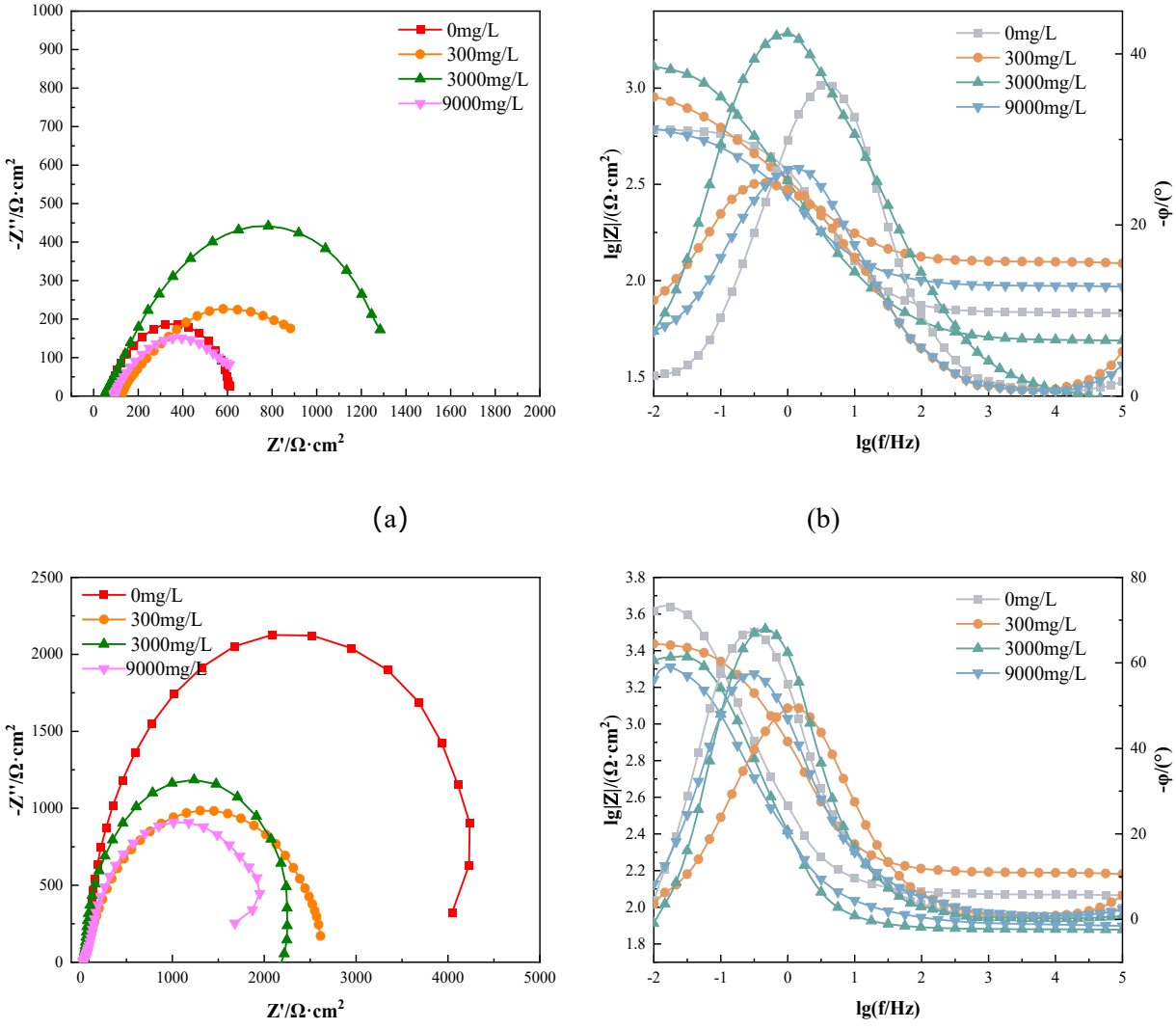


Figure 8. EIS results of L415 pipeline steel after 14 d of immersion in simulated soil solutions with different SO42- concentrations: Nyquist plots (a, c) and Bode plots (b, d) for the sterile (a, b) and SRB-containing (c, d) systems.

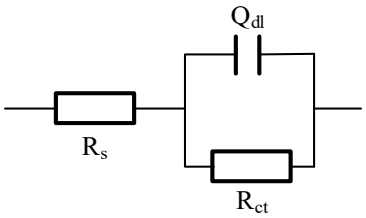


Figure 9. Equivalent circuit models used to fit the EIS data of L415 pipeline steel at different SO_4^{2-} concentrations under SRB-containing and sterile conditions.

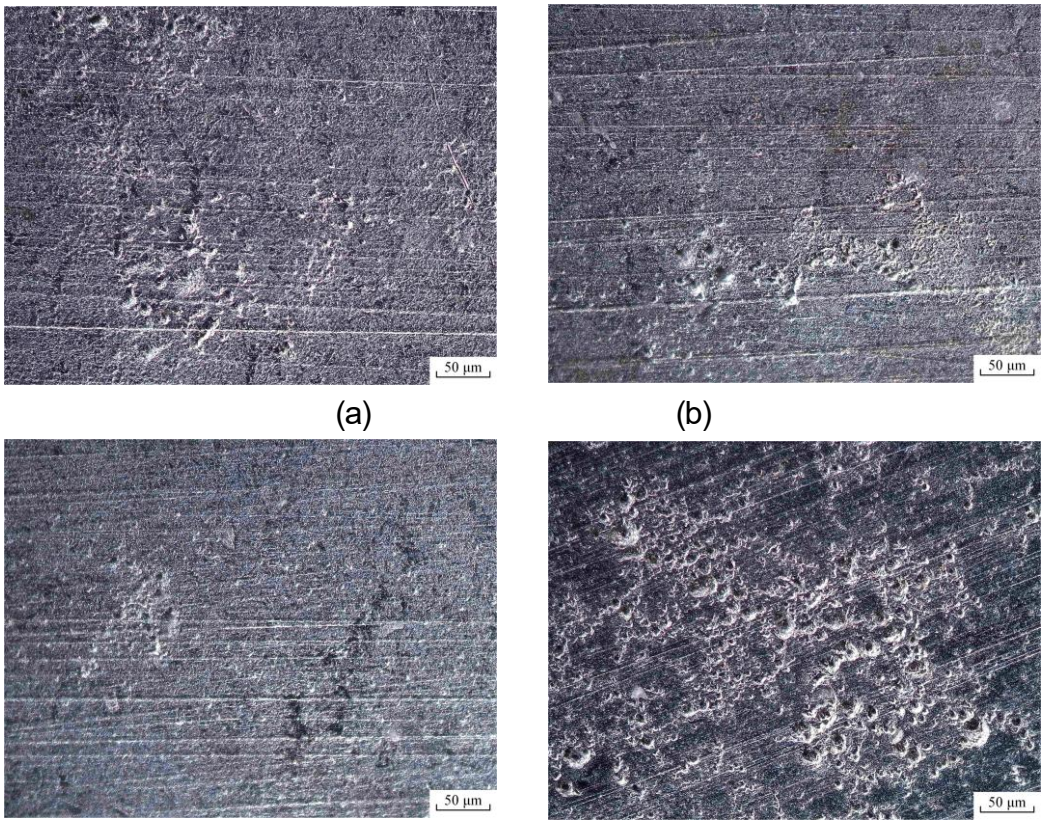
Table 7. Fitted EIS parameters of L415 pipeline steel in sterile and SRB-containing simulated soil solutions with different sulfate concentrations.

	SO_4^{2-} concentration (mg/L)	R_s/(Ω·cm²)	R_{ct}/(Ω·cm²)	R_p/(Ω·cm²)
Sterile	0	68.10	554.3	554.3
	300	122.5	961.8	961.8
	3000	49.17	1519	1519
	9000	93.01	562.4	562.4
SRB	0	38.60	4552.80	4552.80
	300	30.00	2714.03	2714.03
	3000	36.51	2334.33	2334.33
	9000	31.29	2167.06	2167.06

3.4. Corrosion Morphology

Figure 10 and **Figure 11** present the corrosion morphologies of L415 pipeline steel after 14 d of immersion in sterile and SRB-containing simulated soil solutions with different Cl^- concentrations. In the sterile system, scattered pits and localized corrosion clusters were observed at 600 and 3000 mg/L Cl^-, whereas the specimen exposed to 6000 mg/L exhibited a relatively uniform surface with limited pitting. When the Cl^- concentration increased to 12000 mg/L, the pits became denser and locally coalesced, indicating more severe localized corrosion. These morphological changes are consistent with the electrochemical results, in which the sterile system exhibited a high R_p at 6000 mg/L but the highest i_{corr} and lowest R_p at 12000 mg/L.

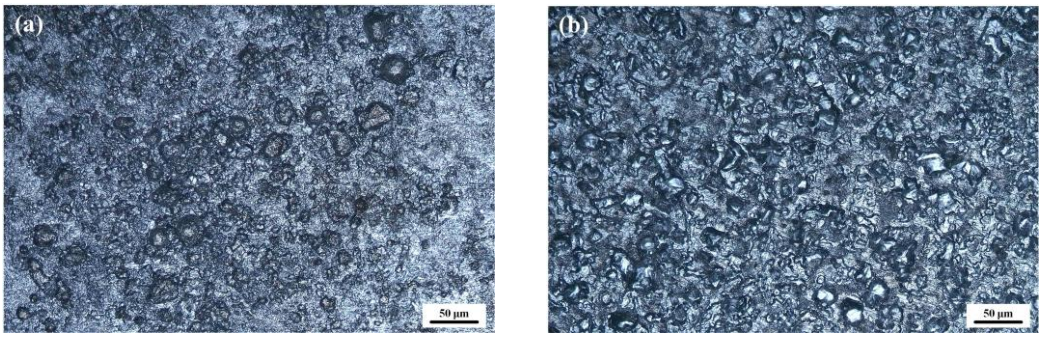
The SRB-containing system showed a different dependence on Cl^- concentration. The most severe pitting occurred at 3000 mg/L, where densely distributed and partially coalesced pits covered the steel surface. As the Cl^- concentration increased to 6000 and 12000 mg/L, the pit density gradually decreased, and the surface became relatively more uniform. This trend agrees with the highest i_{corr} and lowest R_p obtained at 3000 mg/L, as well as the increased R_p at 12000 mg/L. The morphological comparison confirms that moderate Cl^- concentrations promote SRB-associated localized corrosion, whereas the highest Cl^- concentration causes more severe abiotic pitting in the sterile system.



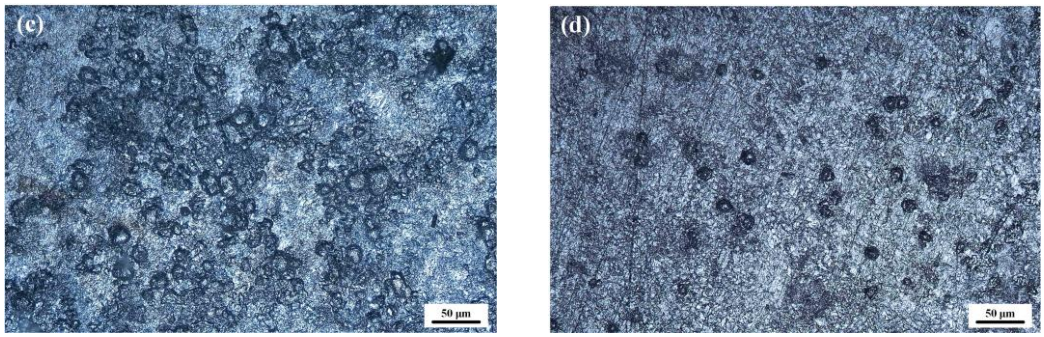
(a) (b)

(c) (d)

Figure 10. Corrosion morphologies of L415 pipeline steel after 14 d of immersion in sterile simulated soil solutions at different Cl^- concentrations: (a) 600, (b) 3000, (c) 6000, and (d) 12000 mg/L.



(a) (b)

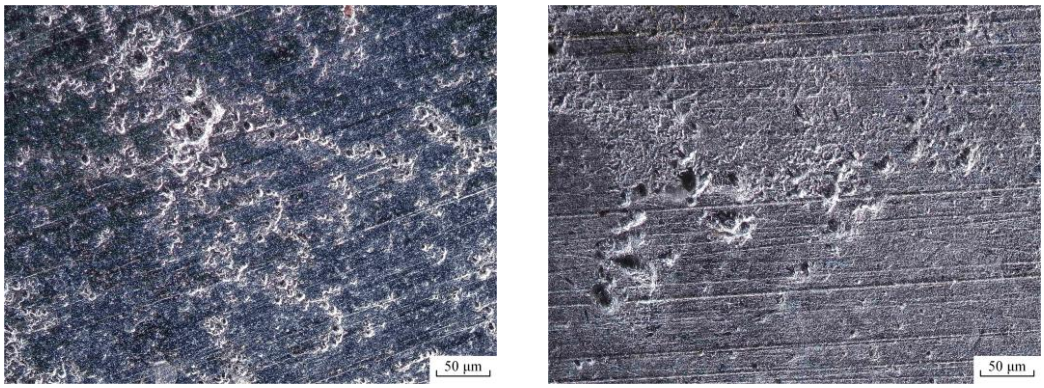


(c) (d)

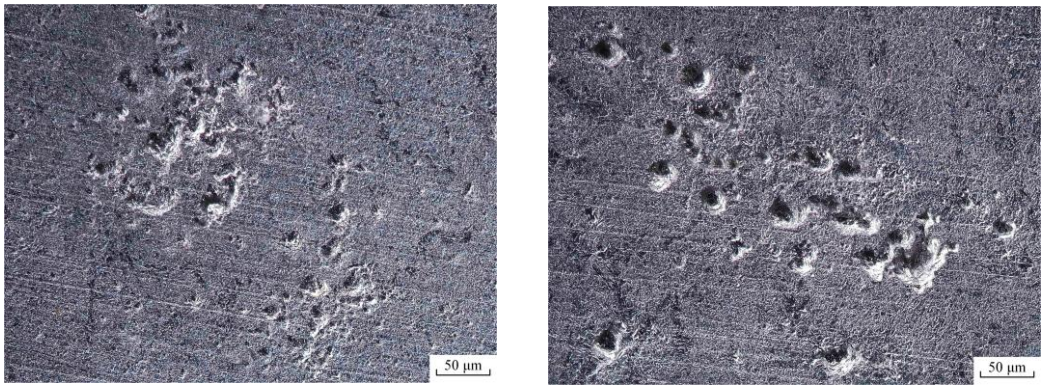
Figure 11. Corrosion morphologies of L415 pipeline steel after 14 d of immersion in SRB-containing simulated soil solutions at different Cl^- concentrations: (a) 600, (b) 3000, (c) 6000, and (d) 12000 mg/L.

Figure 12 and **Figure 13** show the corrosion morphologies of L415 pipeline steel after 14 d of immersion in sterile and SRB-containing simulated soil solutions with different SO_4^{2-} concentrations. In the sterile system, the specimen exposed to the sulfate-free solution exhibited a rough surface with interconnected corrosion patches. Localized corrosion was reduced at 300 mg/L and was least pronounced at 3000 mg/L, where only limited pitting was observed. When the SO_4^{2-} concentration increased to 9000 mg/L, numerous well-defined pits appeared on the surface, indicating a renewed increase in localized corrosion. These observations agree with the electrochemical results, in which the sterile system exhibited the highest R_p and lowest i_{corr} at 3000 mg/L, followed by a decrease in R_p and an increase in i_{corr} at 9000 mg/L.

In the SRB-containing system, the sulfate-free specimen showed a relatively uniform surface with only a few isolated pits. The number and size of the pits increased at 300 and 3000 mg/L, and the most severe pitting was observed at 9000 mg/L, where densely distributed and partially coalesced pits covered the steel surface. This morphology is consistent with the continuous decrease in R_p and the corresponding increase in i_{corr} with increasing SO_4^{2-} concentration. The comparison between the two systems confirms that SO_4^{2-} suppressed localized corrosion at a moderate concentration in the sterile system but progressively promoted SRB-associated pitting corrosion.

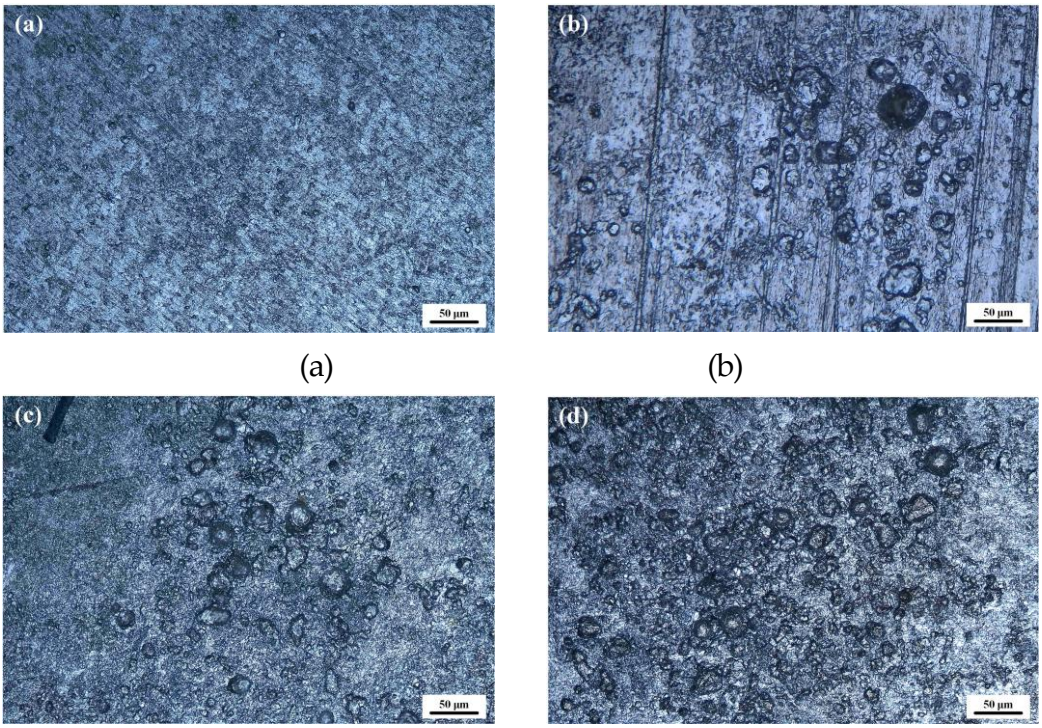


(a) (b)



(c) (d)

Figure 12. Corrosion morphologies of L415 pipeline steel after 14 d of immersion in sterile simulated soil solutions at different SO_4^{2-} concentrations: (a) 0, (b) 300, (c) 3000, and (d) 9000 mg/L.



(a) (b)

(c) (d)

Figure 13. Corrosion morphologies of L415 pipeline steel after 14 d of immersion in SRB-containing simulated soil solutions at different SO_4^{2-} concentrations: (a) 0, (b) 300, (c) 3000, and (d) 9000 mg/L.

4. Conclusions

The corrosion behavior of L415 pipeline steel was governed by the coupled effects of SRB activity, pH, Cl^- concentration, and SO_4^{2-} concentration. Gravimetric measurements showed that the corrosion rate in the sterile system decreased with increasing pH, whereas the SRB-containing system exhibited a maximum corrosion rate near pH 6.6. The inoculated corrosion rate also peaked at 3000 mg/L Cl^- and increased continuously with SO_4^{2-} concentration, while the sterile-reference responses to both ions were non-monotonic.

The correspondence between gravimetric corrosion rates and electrochemical parameters varied with pH. In the sterile system, increasing pH reduced i_{corr} and increased R_p, indicating a continuous improvement in corrosion resistance. In the SRB-containing system, the highest i_{corr} and lowest

R_p occurred at pH 6.6, confirming that near-neutral conditions favored SRB-associated corrosion. At pH 8.0, the lower i_{corr} and higher R_p contrasted with the relatively high cumulative mass loss, suggesting that the final interfacial state measured by electrochemical tests did not fully represent the integrated corrosion process over 14 d.

Chloride concentration produced a transition between SRB-dominated and abiotic corrosion. In the SRB-containing system, the highest i_{corr} and lowest R_p occurred at 3000 mg/L Cl^-, where the metallographic images also showed the most severe pitting. In contrast, the sterile system exhibited its highest i_{corr}, sharply reduced R_p, and severe pit coalescence at 12000 mg/L Cl^-. The inoculated-to-sterile i_{corr} ratio decreased from 15.51 at 3000 mg/L to 0.25 at 12000 mg/L, indicating that moderate chloride enhanced SRB-associated corrosion, whereas chloride-induced abiotic attack dominated at the highest concentration.

SO_4^{2-} exerted contrasting effects in the sterile and SRB-containing systems. In the sterile system, the lowest i_{corr} and highest R_p occurred at 3000 mg/L SO_4^{2-}, followed by renewed corrosion at 9000 mg/L. In the SRB-containing system, i_{corr} increased and R_p decreased continuously with increasing SO_4^{2-} concentration, while pitting became progressively more severe. These results indicate that sulfate availability facilitated SRB metabolism and promoted localized corrosion. The combined gravimetric, electrochemical, and morphological results demonstrate that the corrosion of L415 pipeline steel cannot be interpreted from SRB presence alone but must be evaluated under specific environmental conditions.

Supplementary Materials: Not applicable.

Author Contributions: Yi Liu: conceptualization, methodology, writing-original draft, writing – review and editing, supervision, project administration, funding acquisition. **Fei Li**: writing–review and editing. **Wei Cui**.: writing–review and editing. **Junyi Wei**: investigation.

Funding: This research was funded by the National Science and Technology Major Project for New Oil and Gas Exploration and Development, project “Technology and Equipment for Reconstruction of Oil and Gas Field Production Systems” (grant number 2025ZD1406702).

Data Availability Statement: The data presented in this study are available from the corresponding author upon reasonable request.

Conflicts of Interest: The authors declare no competing financial interest.

Clinical Trial Number: Not applicable.

Ethics, Consent to Participate, and Consent to Publish declarations: Not applicable.

Abbreviations

The following abbreviations are used in this manuscript:

SRB	Sulfate-reducing bacteria
PDP	Potentiodynamic polarization
EIS	Electrochemical impedance spectroscopy
OCP	Open-circuit potential
SCE	Saturated calomel electrode

References

1. Xu, D.; Gu, T.; Lovley, D.R. Microbially mediated metal corrosion. *Nat. Rev. Microbiol.* **2023**, *21*, 705-718. https://doi.org/10.1038/s41579-023-00920-3.

2. Gu, T.; Jia, R.; Unsal, T.; Xu, D. Toward a better understanding of microbiologically influenced corrosion caused by sulfate reducing bacteria. *J. Mater. Sci. Technol.* **2019**, *35*, 631-636. https://doi.org/10.1016/j.jmst.2018.10.026.
3. Jia, R.; Tan, J.L.; Jin, P.; Blackwood, D.J.; Xu, D.; Gu, T. Effects of biogenic H2S on the microbiologically influenced corrosion of C1018 carbon steel by sulfate reducing Desulfovibrio vulgaris biofilm. *Corros. Sci.* **2018**, *130*, 1-11. https://doi.org/10.1016/j.corsci.2017.10.023.
4. Chen, L.; Wei, B.; Xu, X. Effect of Sulfate-Reducing Bacteria (SRB) on the Corrosion of Buried Pipe Steel in Acidic Soil Solution. *Coatings* 2021 11, 625. https://doi.org/10.3390/coatings11060625
5. Liu, W.; Bi, W.; Hu, Y.; Lu, W.; Feng, W.; Wang, Y.; Li, Y.; Liu, J. Influence of initial pH and sulfate-reducing bacteria concentration on the microbiologically influenced corrosion of buried pipeline steel. *Mater. Corros.* **2024**, *75*, 1193-1203. https://doi.org/10.1002/maco.202414320.
6. Wang, L.; Li, J.; Xie, F.; Wang, D.; Wu, M. Anions exacerbate microbial corrosion of X80 pipeline steel induced by sulfate-reducing bacteria in the sea mud environment. *J. Electroanal. Chem.* **2024**, *973*, 118705. https://doi.org/10.1016/j.jelechem.2024.118705.
7. Wang, D.; Ueki, T.; Ma, P.; Xu, D.; Lovley, D.R. Chloride enhances corrosion associated with sulfate-reducing bacteria. *Corros. Sci.* **2024**, *233*, 112096. https://doi.org/10.1016/j.corsci.2024.112096.
8. Zhang, T.; Xu, Z.; Wan, H.; Chen, X.; Liu, H. Dual corrosion promotion of pipeline steel in sea mud induced by sulfate reducing bacteria: Bacteria concentration cell and electronic conduction of the biofilms covered sand grains. *Corros. Sci.* **2024**, *232*, 112005. https://doi.org/10.1016/j.corsci.2024.112005.
9. Li, Y.; Feng, S.; Liu, H.; Tian, X.; Xia, Y.; Li, M.; Xu, K.; Yu, H.; Liu, Q.; Chen, C. Bacterial distribution in SRB biofilm affects MIC pitting of carbon steel studied using FIB-SEM. *Corros. Sci.* **2020**, *167*, 108512. https://doi.org/10.1016/j.corsci.2020.108512.
10. Jin, J.; Guan, Y. The mutual co-regulation of extracellular polymeric substances and iron ions in biocorrosion of cast iron pipes. *Bioresour. Technol.* **2014**, *169*, 387-394. https://doi.org/10.1016/j.biortech.2014.06.059.
11. Jin, J.; Wu, G.; Zhang, Z.; Guan, Y. Effect of extracellular polymeric substances on corrosion of cast iron in the reclaimed wastewater. *Bioresour. Technol.* **2014**, *165*, 162-165. https://doi.org/10.1016/j.biortech.2014.01.117.
12. Li, J.H.; Zhou, E.Z.; Li, Z.; Wang, D.; Wang, F.H.; Xu, D.K. Chloride-dependent enhancement of microbiologically influenced corrosion on X80 steel by Desulfovibrio desulfuricans: The critical role of extracellular polymeric substances. *Pet. Sci.* **2026**, *23*, 2106-2119. https://doi.org/10.1016/j.petsci.2025.12.004.
13. Fu, M.; Cheng, X.; Li, J.; Chen, S.; Dou, W.; Liu, G. Influence of soluble, loosely bound and tightly bound extracellular polymeric substances (EPS) produced by Desulfovibrio vulgaris on EH40 steel corrosion. *Corros. Sci.* **2023**, *221*, 111342. https://doi.org/10.1016/j.corsci.2023.111342.
14. Gao, Y.; Zhang, M.; Fan, Y.; Li, Z.; Cristiani, P.; Chen, X.; Xu, D.; Wang, F.; Gu, T. Marine Vibrio spp. protect carbon steel against corrosion through secreting extracellular polymeric substances. *npj Mater. Degrad.* **2022**, *6*, 6. https://doi.org/10.1038/s41529-022-00216-0.
15. Shangguan, Y.; Liu, M.; Liu, X.; Mei, K.; Shi, B.; Chen, H.; Liao, R.; Liu, K. Sulfate-Reducing Bacteria-Induced Corrosion Behavior of L415 Pipeline Steel in Southern Jiangxi, China. *ACS Omega* **2025**, *10*. 49591-49601, https://doi.org/10.1021/acsomega.5c04172.